American Mineralogist, Volume 83, pages 419–433, 1998

Structural mechanisms of solid solution and cation ordering in augite-jadeite pyroxenes: I. A macroscopic perspective

TIZIANA BOFFA BALLARAN,[1,*] MICHAEL A. CARPENTER,[2] M. CHIARA DOMENEGHETTI,[3] AND VITTORIO TAZZOLI[1]

[1]Dipartimento di Scienze della Terra, Università di Pavia, via Ferrata 1, 27100 Pavia, Italy
[2]Department of Earth Sciences, University of Cambridge, Downing Street, Cambridge CB2 3EQ, U.K.
[3]Centro di studio per la Cristallografia e la Cristallochimica, via Ferrata 1, 27100 Pavia, Italy

ABSTRACT

Single-crystal and powder X-ray diffraction data were collected to characterize the macroscopic solid-solution and cation-ordering behavior in the system augite-jadeite (low acmite content). We examined 28 natural pyroxenes with compositions on the join augite-jadeite and with different degrees of order. Annealing experiments were carried out to obtain crystals with different degrees of order (*P2/n*) and complete disorder (*C2/c*) at compositions between 35 and 60% Jd. Three synthetic *C2/c* pyroxenes with composition $Di_{80}Jd_{20}$, $Di_{60}Jd_{40}$, and $Di_{50}Jd_{50}$ were also examined.

The long-range order parameters Q_{M1} and Q_{M2} of the M1 and M2 sites were obtained by a minimization procedure combining single-crystal X-ray diffraction data and chemical analyses. For both *C2/c* and *P2/n* pyroxenes, the *a, b, c* lattice parameters and unit-cell volume, as well as tetrahedral and octahedral mean bond distances depend linearly on composition. Only the angle β of ordered omphacites slightly deviates from the linear trend of the *C2/c* samples. The out-of-plane tilting of the basal face of tetrahedra is sensitive to the different degrees of order.

INTRODUCTION

The coupled substitution $Ca^{2+} + Mg^{2+}$ $(Fe^{2+}) \leftrightarrow Na^{+} + Al^{3+}$ (Fe^{3+}) along the binary join augite (Aug) $[Ca(Mg,Fe^{2+})Si_2O_6]$-jadeite (Jd) $(NaAl^{3+}\ Si_2O_6)$ [low acmite (Ac) $(NaFe^{3+}\ Si_2O_6)$ content] is known for positive deviations from ideal mixing (Wood et al. 1980; Holland 1983, 1990; Gasparik 1985; Davidson and Burton 1987; Burton and Davidson 1988a, 1988b). It appears that a stability field for the ordered omphacites with *P2/n* symmetry is superimposed on a simple miscibility gap (Carpenter 1980, 1983). The ordering scheme has Mg (Fe^{2+}) and Al (Fe^{3+}) distributed in alternating octahedral sites, M1 (Mg-rich) and M11 (Al-rich), and Na and Ca in the eightfold-coordinated sites, M2 (Na-rich) and M21 (Ca-rich). This scheme may not be followed to its logical limit in that refinements of X-ray single-crystal diffraction data for the most ordered omphacites give complete Mg-Al order, but only partial Ca-Na order, with an average of ¾Ca + ¼Na at M21 and ¾Na + ¼Ca at M2 sites (Rossi et al. 1983; Carpenter et al. 1990a, 1990b). Understanding the factors responsible for the positive deviation from ideality in *C2/c* sodic pyroxenes, the apparently contradictory effects of exsolution and ordering, and the mechanisms by which the cations with different size and charge are accommodated in the pyroxenes structure requires knowledge of the microscopic behavior of the solid-solution augite-jadeite. Spectroscopic methods, with their short characteristic length scale, may resolve these issues and reveal the true local state of cation order that gives the incomplete order observed at length scale characteristic of X-ray diffraction.

Accordingly, X-ray diffraction (part I) and IR spectroscopic (part II; Boffa Ballaran et al. 1998) studies have been carried out on several sodic pyroxenes, with different compositions and degrees of order, to investigate both macroscopic and microscopic mixing behavior of the solid-solution Aug-Jd and to define the short-range order parameters in omphacites. For the purpose of these papers we use the convention that microscopic means the local scale examined by IR spectroscopy and macroscopic means the average structure as determined by X-ray diffraction.

EXPERIMENTAL METHODS

Samples

Sodic pyroxenes were chosen to obtain compositions representative of the binary join Aug-Jd. A list of the samples investigated and references are given in Table 1. Three synthetic pyroxenes investigated by Wood et al. (1980) and Holland (1983) with composition $Di_{80}Jd_{20}$, $Di_{60}Jd_{40}$, and $Di_{50}Jd_{50}$ (*C2/c* structure) were analyzed by X-ray powder diffraction due to small grain size.

Annealing experiments

Annealing experiments were carried out to obtain different degrees of order in crystals of the same composi-

* Present address: Department of Earth Sciences, University of Cambridge, Downing Street, Cambridge CB2 3EQ, U.K. E-mail: tiziana@esc.cam.ac.uk

0003–004X/98/0506–04190$05.00

TABLE 1. Space groups, localities, rock and mineral types, and references of the investigated pyroxenes

Sample	Space group	Locality	Rock or mineral type	Reference
Diopside	*C2/c*	Dekalb County, New York	Diopside	[1]
ML	*C2/c*	Macchie, Italy	Phonolite	[2]
N16/2	*C2/c*	Sonnemore Norway	Garnet pyroxenite	[3]
C411	*C2/c*	Nybö Norway	Eclogite	[4]
C413A	*C2/c*	Nybö Norway	Eclogite	[4]
C413B	*C2/c*	Nybö Norway	Eclogite	[4]
C413C	*C2/c*	Nybö Norway	Eclogite	[4]
74AM43	*C2/c*	Münchberg Mass Bavaria	Eclogite	[5]
74AM39	*C2/c*	Münchberg Mass Bavaria	Eclogite	[5]
74AM40	*P2/n*	Münchberg Mass Bavaria	Eclogite	[5]
74AM41	*P2/n*	Münchberg Mass Bavaria	Eclogite	[5]
74AM42	*P2/n*	Münchberg Mass Bavaria	Eclogite	[5]
74AM33	*P2/n*	Münchberg Mass Bavaria	Eclogite	[5]
78AM12	*P2/n*	Val Mesolcina Soazza	Eclogite	[6]
MS1	*P2/n*	Isasca Dora-Maira	Phengite eclogite	[7]
Ma4	*P2/n*	Martiniana Dora-Maira	Amphibole phengite eclogite	[7]
Br2	*P2/n*	Brossasco Dora-Maira	Horneblende phengite eclogite	[8]
MfX	*P2/n*	Brossasco Dora-Maira	Phengite eclogite	[7]
M106	*P2/n*	Oropa Sesia-Lanzo	Amphibole eclogite	[9]
SL988	*P2/n*	Quassolo Sesia-Lanzo	Glaucophane phengite omphacitite	[7]
SL896	*P2/n*	Brosso Sesia-Lanzo	Glaucophane omphacitite	[10]
SL993	*P2/n*	Quassolo Sesia-Lanzo	Garnet glaucophane omphacitite	[7]
SL986	*C2/c*	Quassolo Sesia-Lanzo	Jadeitite	[11]
SL504	*C2/c*	Settimo Vittone Sesia-Lanzo	Jadeite micaschist	[10]
SL664	*C2/c*	Quincinetto Sesia-Lanzo	Meta-aplite dyke	[10]
SLVD1	*C2/c*	Le Colme	Jadeite megablast	[12]
120853	*P2/n*	Tauern region	Kyanite eclogite	[13]
NI2	*C2/c*	New Idria	Jadeite	[14]

Note: [1] Mineral collection Dept. of Earth Sciences Cambridge; [2] Stoppa and Lavecchia (1992); [3] Medaris (1980); [4] Lappin and Smith (1978); [5] Matthes and Schmidt (1974); [6] Aurisicchio et al. (1985); [7] Boffa Ballaran and Domeneghetti (1996); [8] Kienast et al. (1991); [9] Ungaretti et al. (1983); [10] Lombardo et al. (1977); [11] kindly provided by B. Lombardo; [12] kindly provided by R. Compagnoni; [13] Carpenter (1981); [14] Coleman (1961).

TABLE 2. Electron microprobe analyses

	ML	Diopside	N16/2	C411	74AM43	74AM39	74AM40	78AM12	74AM41
					Weight percentages				
SiO_2	53.62(39)	56.03(15)	55.12(20)	55.80(18)	55.26(46)	56.24(27)	56.51(32)	55.75(27)	56.40(24)
TiO_2	0.32(5)	0.02(2)	0.09(5)	0.07(3)	0.09(4)	0.12(4)	0.16(3)	0.11(5)	0.12(4)
Al_2O_3	1.80(42)	0.37(5)	1.82(18)	1.25(14)	6.04(25)	8.76(18)	9.23(21)	8.01(47)	10.74(12)
Cr_2O_3	0.60(25)	0.08(4)	0.38(7)	0.10(5)	0.12(6)	0.23(13)	0.25(18)	0.12(6)	0.14(7)
FeO	2.89(41)	1.02(13)	2.32(15)	4.02(12)	1.34(9)	1.89(8)	2.04(10)	4.20(18)	2.46(9)
MnO	0.06(5)	0.03(4)	0.04(4)	0.02(2)	0.03(3)	0.02(3)	0.01(2)	0.04(4)	0.03(4)
MgO	16.66(31)	17.66(14)	16.17(15)	15.69(14)	13.48(19)	11.28(13)	10.88(23)	10.61(29)	9.32(10)
CaO	24.11(30)	25.97(11)	22.76(18)	22.80(19)	19.29(52)	17.32(16)	16.89(13)	15.74(20)	14.94(10)
Na_2O	0.13(2)	0.41(1)	1.54(7)	1.41(9)	3.57(11)	5.07(11)	5.53(10)	5.54(21)	6.59(12)
K_2O	0.01(1)	0.00(1)	0.00(1)	0.02(1)	0.00(1)	0.01(1)	0.00(1)	0.01(1)	0.01(1)
Total	100.20(22)	101.59(26)	100.24(36)	101.18(33)	99.22(83)	100.94(41)	101.50(59)	100.13(35)	100.75(32)
Si	1.952(9)	1.998(4)	1.993(4)	2.010(3)	1.987(4)	1.982(4)	1.980(3)	1.996(4)	1.985(2)
Ti	0.009(2)	0.001(1)	0.002(1)	0.002(1)	0.002(1)	0.003(1)	0.004(1)	0.003(1)	0.003(1)
Al	0.077(18)	0.015(2)	0.078(8)	0.053(6)	0.256(11)	0.364(6)	0.381(8)	0.338(19)	0.445(5)
Cr	0.017(7)	0.002(1)	0.011(2)	0.003(1)	0.003(2)	0.006(4)	0.007(5)	0.003(2)	0.004(2)
Fe^{2+}	0.088(13)	0.017(4)	0.051(8)	0.076(5)	0.040(3)	0.056(9)	0.060(5)	0.080(12)	0.068(7)
Fe^{3+}	0.000(4)	0.013(3)	0.019(6)	0.045(5)	0.000(9)	0.000(7)	0.000(4)	0.046(13)	0.004(5)
Mn	0.002(2)	0.001(1)	0.001(1)	0.000(1)	0.001(1)	0.001(1)	0.000(1)	0.001(1)	0.001(1)
Mg	0.903(14)	0.938(6)	0.871(6)	0.842(7)	0.723(13)	0.592(7)	0.568(11)	0.566(16)	0.489(5)
Ca	0.940(12)	0.992(4)	0.881(8)	0.880(8)	0.743(16)	0.654(8)	0.634(6)	0.604(10)	0.563(3)
Na	0.009(2)	0.028(1)	0.108(5)	0.098(6)	0.249(9)	0.346(7)	0.376(6)	0.384(14)	0.449(9)
K	0.000(1)	0.000(0)	0.000(0)	0.001(1)	0.000(0)	0.000(1)	0.000(1)	0.000(1)	0.000(0)
Total	3.997(2)	4.005(4)	4.015(3)	4.010(4)	4.004(7)	4.004(3)	4.010(4)	4.021(6)	4.011(4)
Aug	100.00	97.44	90.08	89.98	74.37	64.24	62.46	61.13	55.63
Ac	0.00	1.28	1.94	4.60	0.00	0.00	0.00	4.66	0.40
Jd	0.00	1.28	7.98	5.42	25.63	35.76	37.54	34.21	43.97
X_{Jd+Ac}	0.000	0.026	0.099	0.100	0.256	0.358	0.375	0.389	0.444

TABLE 2—*Continued*

	MS1	74AM42	Ma4	120853	M106	74AM33	MfX	Br2	SL988
					Weight percentages				
SiO_2	56.96(36)	56.40(39)	56.57(21)	56.73(23)	56.49(38)	57.33(29)	56.73(34)	56.64(29)	56.59(25)
TiO_2	0.08(3)	0.14(7)	0.08(3)	0.08(7)	0.11(6)	0.13(6)	0.08(4)	0.09(4)	0.08(4)
Al_2O_3	10.87(39)	10.79(10)	10.31(61)	11.78(29)	11.88(54)	12.77(21)	12.57(48)	12.54(42)	12.51(69)
Cr_2O_3	0.19(5)	0.15(6)	0.17(12)	0.08(8)	0.08(5)	0.07(3)	0.09(5)	0.06(4)	0.08(7)
FeO	1.34(9)	2.43(6)	3.57(19)	2.07(18)	2.93(39)	2.30(7)	2.79(36)	2.97(45)	4.50(75)
MnO	0.02(2)	0.01(1)	0.04(4)	0.03(3)	0.02(2)	0.03(2)	0.02(3)	0.03(4)	0.04(3)
MgO	9.65(25)	9.26(6)	8.82(44)	8.84(36)	8.40(22)	8.03(12)	7.59(25)	7.72(17)	6.79(32)
CaO	14.87(37)	14.75(11)	13.84(43)	13.05(45)	12.69(45)	12.93(19)	12.15(48)	12.09(28)	11.24(60)
Na_2O	6.58(25)	6.60(14)	6.60(29)	7.34(23)	7.56(36)	7.90(11)	7.55(31)	7.86(22)	7.94(34)
K_2O	0.01(1)	0.01(2)	0.01(1)	0.02(2)	0.01(2)	0.01(2)	0.01(1)	0.01(2)	0.03(5)
Total	100.57(35)	100.54(51)	100.01(40)	100.02(54)	100.17(52)	101.50(30)	99.58(37)	100.01(32)	99.80(35)
Si	1.995(4)	1.987(5)	2.008(4)	1.996(6)	1.992(4)	1.989(5)	2.003(5)	1.996(4)	2.007(4)
Ti	0.002(1)	0.004(2)	0.002(1)	0.002(2)	0.003(2)	0.003(1)	0.002(1)	0.002(1)	0.002(1)
Al	0.449(14)	0.448(3)	0.431(25)	0.488(13)	0.494(20)	0.522(8)	0.523(18)	0.521(16)	0.523(28)
Cr	0.005(1)	0.004(2)	0.005(3)	0.002(2)	0.002(1)	0.002(1)	0.002(1)	0.002(1)	0.002(2)
Fe^{2+}	0.039(3)	0.069(9)	0.083(11)	0.048(9)	0.063(16)	0.058(6)	0.082(13)	0.072(15)	0.110(17)
Fe^{3+}	0.000(1)	0.003(8)	0.023(11)	0.013(9)	0.023(10)	0.009(7)	0.000(7)	0.016(9)	0.023(11)
Mn	0.001(1)	0.000(0)	0.001(1)	0.001(1)	0.001(1)	0.001(1)	0.001(1)	0.001(1)	0.001(1)
Mg	0.503(15)	0.486(3)	0.466(23)	0.463(18)	0.441(13)	0.415(6)	0.399(14)	0.405(10)	0.359(17)
Ca	0.558(16)	0.557(5)	0.526(17)	0.492(15)	0.479(19)	0.480(8)	0.460(20)	0.456(12)	0.427(24)
Na	0.447(16)	0.451(8)	0.454(20)	0.501(17)	0.517(22)	0.531(8)	0.517(19)	0.537(13)	0.546(22)
K	0.000(0)	0.000(1)	0.000(1)	0.001(1)	0.000(1)	0.000(1)	0.000(1)	0.000(1)	0.001(2)
Total	3.999(5)	4.009(7)	3.999(4)	4.007(6)	4.015(6)	4.010(6)	3.989(5)	4.008(4)	4.001(6)
Aug	55.41	55.26	53.67	49.55	48.09	47.48	46.80	45.92	43.88
Ac	0.00	0.30	2.35	1.31	2.31	0.89	0.00	1.61	2.36
Jd	44.59	44.44	43.98	49.14	49.60	51.63	53.20	52.47	53.75
X_{Jd+Ac}	0.446	0.447	0.463	0.504	0.519	0.525	0.532	0.541	0.561

TABLE 2—*Continued*

	SL896	SL993	C413A	C413C	C413B	SL986	SL504	SLVD1	SL664	NI2
					Weight percentages					
SiO_2	56.43(35)	56.71(45)	57.80(45)	57.49(18)	58.11(11)	58.33(31)	58.44(32)	58.78(31)	59.30(26)	58.93(29)
TiO_2	0.10(5)	0.09(5)	0.11(5)	0.14(4)	0.18(2)	0.04(3)	0.05(4)	0.01(2)	0.03(3)	0.02(3)
Al_2O_3	12.90(99)	13.07(99)	16.08(92)	17.18(68)	17.35(11)	20.93(80)	21.51(63)	23.04(21)	24.08(12)	24.79(38)
Cr_2O_3	0.08(5)	0.09(7)	0.03(2)	0.02(2)	0.02(2)	0.03(3)	0.02(2)	0.02(2)	0.01(2)	0.03(3)
FeO	5.50(46)	4.22(77)	3.73(9)	3.73(13)	3.72(9)	3.50(58)	2.95(44)	2.39(29)	1.43(23)	0.26(25)
MnO	0.04(3)	0.02(2)	0.04(2)	0.03(3)	0.04(2)	0.05(2)	0.07(4)	0.02(3)	0.02(2)	0.02(3)
MgO	5.95(54)	6.53(49)	4.76(55)	3.81(40)	3.86(19)	0.95(28)	0.86(28)	0.04(4)	0.02(3)	0.01(3)
CaO	10.93(99)	10.78(99)	6.68(82)	5.27(59)	5.33(23)	2.20(52)	1.78(48)	0.55(14)	0.37(13)	0.06(4)
Na_2O	8.10(63)	8.22(66)	10.57(45)	11.30(37)	11.58(12)	13.41(44)	13.33(29)	14.28(10)	14.83(11)	15.11(20)
K_2O	0.01(1)	0.00(1)	0.01(1)	0.00(1)	0.01(1)	0.01(3)	0.01(1)	0.01(1)	0.03(9)	0.00(1)
Total	100.04(39)	99.73(33)	99.81(49)	98.97(16)	100.20(21)	99.45(39)	99.02(29)	99.14(41)	100.12(37)	99.23(51)
Si	2.004(4)	2.007(4)	2.018(3)	2.017(5)	2.015(5)	2.017(4)	2.019(5)	2.017(4)	2.007(3)	2.001(9)
Ti	0.003(1)	0.002(1)	0.003(1)	0.004(1)	0.005(1)	0.001(1)	0.001(1)	0.000(0)	0.001(1)	0.001(1)
Al	0.540(43)	0.545(47)	0.661(35)	0.710(27)	0.709(5)	0.853(29)	0.876(22)	0.932(7)	0.960(4)	0.992(12)
Cr	0.002(1)	0.003(2)	0.001(1)	0.001(1)	0.001(0)	0.001(1)	0.001(1)	0.001(1)	0.000(1)	0.001(1)
Fe^{2+}	0.146(12)	0.106(19)	0.055(13)	0.051(7)	0.039(6)	0.055(16)	0.068(13)	0.051(9)	0.027(10)	0.005(6)
Fe^{3+}	0.017(10)	0.019(12)	0.054(15)	0.058(10)	0.069(8)	0.046(13)	0.017(12)	0.018(9)	0.013(7)	0.002(7)
Mn	0.001(1)	0.001(1)	0.001(1)	0.001(1)	0.001(1)	0.001(1)	0.002(1)	0.001(1)	0.001(1)	0.001(1)
Mg	0.315(30)	0.344(28)	0.248(30)	0.199(21)	0.199(9)	0.049(15)	0.044(15)	0.002(2)	0.001(2)	0.001(1)
Ca	0.416(42)	0.409(43)	0.250(32)	0.198(22)	0.198(8)	0.081(19)	0.066(18)	0.020(5)	0.013(5)	0.002(1)
Na	0.557(40)	0.564(41)	0.715(29)	0.768(25)	0.778(8)	0.899(27)	0.893(17)	0.950(8)	0.973(7)	0.994(10)
K	0.000(1)	0.000(0)	0.000(1)	0.000(0)	0.000(1)	0.000(1)	0.000(1)	0.000(0)	0.001(4)	0.000(1)
Total	4.001(4)	4.000(7)	4.006(8)	4.007(6)	4.014(6)	4.003(7)	3.987(6)	3.992(4)	3.997(5)	4.000(8)
Aug	42.75	42.04	25.90	20.50	20.29	8.27	6.88	2.06	1.32	0.20
Ac	1.75	1.95	5.60	6.00	7.07	4.69	1.77	1.86	1.32	0.20
Jd	55.50	56.01	68.50	73.50	72.64	87.04	91.35	96.08	97.36	99.60
X_{Jd+Ac}	0.572	0.580	0.741	0.795	0.797	0.917	0.931	0.979	0.987	0.998

Note: Standard deviations are in parentheses, and in calculating Fe^{2+}/Fe^{3+} and Aug, Ac, Jd proportions it has been assumed that all the Al is in the octahedral sites and the tetrahedral sites are fully occupied by Si.

* Only this sample contains tetrahedral Al. This could be expressed in terms of a CaTs component (~5 mol%), but is included in the Aug fraction for present purposes.

TABLE 4a. Refinement data from X-ray single-crystal diffraction for *C2/c* pyroxenes

	I_{tot}	I	R_{int} (%)	R (%)	wR (%)	S	m.a.n. of M1	m.a.n. of M2	m.a.n. of M2′
ML n.3	1349	651	1.73	1.32	3.69	1.174	14.88(3)	19.62(5)	0.40(5)
ML n.4	1361	649	1.52	1.54	4.17	1.208	13.75(3)	19.38(5)	0.70(5)
Diopside	1366	652	1.78	1.78	4.67	1.206	12.39(4)	19.78(4)	
N16/2 n.3	1348	646	0.80	1.29	3.26	1.152	12.90(3)	18.74(5)	0.42(5)
C411g n.1	1345	646	1.01	1.41	3.91	1.142	13.43(3)	18.86(5)	0.54(5)
74AM43 n.1	1319	638	1.34	1.52	3.87	1.157	12.77(3)	17.89(4)	
74AM43 n.2	1320	634	1.11	1.44	3.59	1.104	12.72(3)	17.56(5)	0.27(5)
74AM39 n.1	1299	628	1.02	1.45	3.89	1.185	13.12(3)	16.80(5)	0.27(6)
74AM40 168h	2317	625	2.00	1.70	4.44	1.104	13.28(3)	16.49(4)	
74AM33 458h	2286	616	0.95	1.62	4.26	1.198	13.31(3)	14.99(4)	
C413A n.1	1265	605	0.88	1.48	3.92	1.176	13.89(3)	12.94(4)	
C413C n.2	1250	601	1.42	1.48	3.96	1.104	13.91(3)	12.67(4)	
C413B n.1	1263	600	0.68	1.36	3.65	1.203	13.94(3)	12.68(4)	
SL986 n.1	1215	590	0.95	1.34	3.29	1.055	14.13(3)	11.34(4)	
SL504 n.2	1217	590	1.26	1.34	3.48	1.084	13.84(3)	11.05(4)	
SLVD1 n.2	1207	588	1.26	1.55	4.19	1.077	13.80(3)	10.93(3)	
SL664 n.2	1418	587	1.31	1.47	3.72	1.183	13.63(3)	10.86(4)	
NI2 n.1	1229	587	0.66	1.60	4.04	1.132	13.04(3)	10.93(4)	

Note: Standard deviations are in parentheses.

I_{tot} = number of total reflections; I = number of unique reflections; m.a.n. = mean atomic number,

$$R_{int} = \sum |F_o^2 - \bar{F}_o^2| \Big/ \sum |F_o^2 \quad R = \sum ||F_o| - |F_c|| \Big/ \sum |F_o| \text{ for } F_o^2 > 2\sigma(F_o^2) \quad wR = \left[\sum w(F_o^2 - F_c^2)^2 \Big/ \sum w(F_o^2)^2\right]^{1/2}$$

$$S = \left[\sum w(F_o^2 - F_c^2)^2 \Big/ (n - p)\right]^{1/2} \text{ where } n = \text{number of the reflections and } p = \text{total number of parameters refined.}$$

tion and to generate completely disordered (*C2/c*) omphacites with compositions between 35 and 60% Jd (the composition range of ordered *P2/n* omphacite). Five 20 mg samples of crystals from 74AM33 were heated in evacuated silica tubes at 950 °C for 2.5, 10, 45, and 458 h. The same amount of sample from 74AM40 was experimentally disordered in an evacuated silica tube at 900 °C for 168 h. After the annealing, no change in color or transparency of the crystals was observed, suggesting that little (if any) oxidation or alteration had occurred. For samples MS1, 74AM42, Ma4, Br2, and SL896, high pressure was needed to suppress the breakdown reaction of omphacite to a mixture of plagioclase feldspar, nepheline, and a more Ca-rich pyroxene. The disordering process was therefore carried out with ~10 mg of crystals in platinum containers at 1000 °C and 20 kbar for 6 h. Crystals of samples N16/2 and SL986 (~10 mg each), both with *C2/c* structures, were treated at 1000 °C and 20 kbar for 6 h in platinum containers to allow comparison of disordered crystals equilibrated at high temperature with those equilibrated at relatively low temperature during slow cooling in nature. The products from high-pressure experiments were not suitable for X-ray single-crystal diffraction.

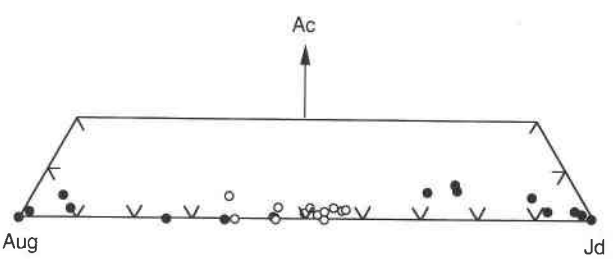

FIGURE 1. Compositions of the investigated pyroxenes in the ternary system augite-jadeite-acmite. Filled circles = *C2/c* samples; open circles = *P2/n* samples.

Electron microprobe analysis

Compositions were determined by electron microprobe analysis (CAMECA SX50), operating at 20 kV with a 15 nA sample current. All elements (except Na) were determined by energy dispersive analysis using a Link AN10000 system with ZAF4/FSL quantitative software. Na was determined by wavelength dispersive analysis using jadeite as the standard. Up to 20 point analyses were obtained from several crystals of each sample. Fe^{3+} and Fe^{2+} were calculated assuming $Fe^{3+} = Na - {}^{[6]}Al$ and $Fe^{2+} = Fe_{tot} - Fe^{3+}$. The average compositions obtained are given in Table 2.

Augite, acmite, and jadeite proportions were recalculated to 100% from Aug = Ca, Ac = Fe^{3+}, Jd = $^{[6]}Al$. For present purposes, the Ac content (which never exceeds 7%) was included in the mole fraction of the jadeite component. The variation in composition of the investigated samples is described in term of X_{Jd+Ac} (Table 2) and the range of compositions is shown in Figure 1.

X-ray single-crystal diffraction

X-ray diffraction data were collected using a Philips PW1100 four-circle automated diffractometer with graphite monochromated Mo$K\alpha$ radiation. The equivalent pairs hkl and $h\bar{k}l$ were measured in the θ range 2–30° using the ω-scan mode. Net X-ray diffraction intensities were de-

TABLE 4b. Refinement data from X-ray single-crystal diffraction for *P2/n* pyroxenes

	I_{tot}	I	R_{int} (%)	R (%)	wR (%)	S	m.a.n. of M11	m.a.n. of M1	m.a.n. of M2	m.a.n. of M21
74AM40 n.1	2493	1253	1.45	2.09	5.86	1.052	13.55(4)	12.95(4)	15.50(4)	17.66(4)
78AM12 n.2	2553	1263	1.33	1.61	4.58	1.024	14.13(3)	13.54(3)	15.17(4)	17.76(4)
78AM12 n.3	2534	1258	0.98	1.77	5.22	1.064	14.10(3)	13.48(3)	15.13(3)	17.70(3)
74AM41 n.1	2522	1251	1.26	1.72	4.64	1.038	13.51(3)	13.21(3)	13.96(4)	17.84(4)
74AM41 n.2	2497	1248	1.30	1.81	4.90	1.035	13.41(4)	13.12(4)	13.83(5)	17.73(5)
MS1 n.3	2527	1251	1.32	1.83	5.11	1.090	13.24(3)	12.70(3)	14.20(4)	17.88(4)
74AM42 n.1	2521	1244	2.13	1.91	5.29	1.075	13.50(3)	13.21(3)	13.97(4)	17.86(4)
Ma4 n.1	2464	1249	1.45	1.79	4.71	1.055	13.79(4)	13.72(4)	13.22(5)	17.83(5)
Ma4 n.2	2493	1248	1.57	1.86	4.69	1.027	13.65(4)	13.82(4)	13.08(5)	17.62(5)
120853 n.5	2533	1247	1.67	2.25	6.58	1.081	13.44(3)	12.99(3)	13.30(5)	17.69(5)
M106 n.2	2495	1240	1.09	1.61	5.06	1.204	13.46(4)	13.58(4)	12.88(5)	17.63(5)
M106 n.4	2563	1241	1.03	1.68	4.65	1.133	13.38(3)	13.48(3)	12.88(4)	17.53(4)
74AM33 n.11	2532	1239	1.45	2.25	6.57	1.147	13.20(4)	13.29(4)	13.10(5)	17.24(5)
74AM33 n.17	2519	1243	1.21	1.91	4.96	1.121	13.21(3)	13.19(3)	12.97(4)	17.26(4)
74AM33 2.5h	2428	1233	0.95	1.63	4.81	1.048	13.55(3)	13.16(3)	13.86(4)	16.21(4)
74AM33 10h	2396	1239	1.28	2.11	6.95	1.030	13.59(5)	13.07(5)	14.54(6)	15.55(6)
74AM33 45h	2347	1237	1.02	1.81	5.37	1.090	13.61(5)	13.04(5)	14.81(6)	15.44(6)
MfX n.1	2475	1234	1.16	1.97	5.34	1.060	13.41(3)	13.57(3)	12.83(4)	16.98(4)
MfX n.4	2482	1237	0.92	1.52	4.40	1.056	13.42(3)	13.65(3)	12.78(4)	17.11(4)
Br2 n.10	2518	1240	0.92	1.74	4.90	1.141	13.30(3)	13.61(3)	12.68(4)	17.14(4)
Br2 n.11	2534	1237	1.01	1.80	5.16	1.130	13.30(3)	13.60(3)	12.73(4)	17.21(4)
SL988 n.1	2466	1242	1.49	2.53	7.04	1.167	13.76(7)	14.95(7)	12.74(9)	17.07(9)
SL896 n.3	2459	1231	1.83	2.65	7.29	1.102	13.78(6)	15.31(6)	12.74(7)	16.19(7)
SL993 n.1	2482	1232	2.45	3.44	9.93	1.293	13.63(9)	14.76(9)	12.52(11)	16.15(11)

Note: Standard deviations are in parentheses. I, R_{int}, R, wR, S, and m.a.n. as in Table 4a.

termined by measuring step-scan profiles and analyzing them by the Lehman-Larsen (1974) $\sigma(I)/I$ method, modified by Blessing et al. (1974). Details of the analyzed crystals and of the data collection (Table 3[1]) have been deposited. For ordered omphacites, the weak *hkl* reflections with $h + k = 2n + 1$ (class *b* reflections) that disappear in disordered *C2/c* omphacites, were always present, confirming *P2/n* symmetry. The intensities were corrected for absorption following the Ψ scan method of North et al. (1968). The unit-cell parameters were determined by using a locally improved version of the Philips LAT routine (Cannillo et al. 1983) on 50–60 reflections.

Structure refinements based on F_o^2 were performed using the program SHELXL93 (Sheldrick 1993). The values of equivalent pairs were averaged and the resulting discrepancy factors $R_{int} = \Sigma|F_o^2 - \overline{F_o^2}|/\Sigma F_o^2$ are reported in Tables 4a and 4b for *C2/c* and *P2/n* pyroxenes, respec-

[1] For a copy of Tables 3, 6, and 7, Document AM-98-010, contact the Business Office of the Mineralogical Society of America (see inside front cover of recent issue) for price information. Deposit items may also be available on the *American Mineralogist* web site at http://www.minsocam.org.

TABLE 5a. Mean bond distances (Å), volume (Å³) of M1 polyhedron, and other geometrical parameters* of tetrahedra for *C2/c* pyroxenes

	⟨Si-O⟩	⟨M1-O⟩	⟨M2-O⟩	⟨M2′-O⟩	V_{M1}	TQE	TAV	TILT	$TILT_{az}Si1$	$TILT_{az}Si2$	O3-O3-O3
ML n.3	1.649(1)	2.068(1)	2.495(1)	2.543(1)	11.693	1.0062	26.12	2.462	187.1	−7.1	165.72
ML n.4	1.641(1)	2.077(1)	2.496(1)	2.544(1)	11.845	1.0062	26.15	2.545	187.1	−7.1	165.72
Diopside	1.635(1)	2.077(1)	2.500(1)		11.851	1.0066	28.04	2.516	186.8	−6.8	166.44
N16/2 n.3	1.634(1)	2.069(1)	2.497(1)	2.544(1)	11.706	1.0062	26.56	2.436	186.6	−6.6	166.71
C411g n.1	1.634(1)	2.071(1)	2.497(1)	2.544(1)	11.748	1.0062	26.49	2.475	186.7	−6.7	166.62
74AM43 n.1	1.633(1)	2.042(1)	2.492(1)		11.230	1.0059	25.43	2.212	186.1	−6.1	167.82
74AM43 n.2	1.633(1)	2.040(1)	2.492(1)	2.539(1)	11.210	1.0059	25.46	2.223	186.1	−6.1	167.85
74AM39 n.1	1.633(1)	2.024(1)	2.489(1)	2.535(1)	10.924	1.0058	24.89	2.120	185.7	−5.7	168.65
74AM40 168h	1.631(1)	2.022(1)	2.489(1)		10.890	1.0056	24.24	2.007	185.6	−5.6	168.73
74AM33 458h	1.630(1)	1.999(1)	2.486(1)		10.502	1.0055	23.52	1.902	185.0	−5.0	170.01
C413A n.1	1.627(1)	1.969(1)	2.480(1)		10.004	1.0052	22.20	1.749	183.9	−3.9	172.23
C413C n.2	1.626(1)	1.966(1)	2.480(1)		9.955	1.0052	22.30	1.798	183.7	−3.7	172.52
C413B n.1	1.627(1)	1.966(1)	2.480(1)		9.946	1.0053	22.32	1.743	183.7	−3.7	172.52
SL986 n.1	1.625(1)	1.946(1)	2.476(1)		9.632	1.0053	22.25	1.702	183.1	−3.1	173.79
SL504 n.2	1.625(1)	1.942(1)	2.475(1)		9.566	1.0053	22.18	1.684	183.0	−3.0	174.04
SLVD1 n.2	1.624(1)	1.936(1)	2.472(1)		9.469	1.0054	22.58	1.672	182.8	−2.8	174.39
SL664 n.2	1.625(1)	1.935(1)	2.473(1)		9.456	1.0054	22.48	1.689	182.8	−2.8	174.46
NI2 n.1	1.625(1)	1.930(1)	2.470(1)		9.393	1.0055	22.78	1.669	182.7	−2.7	174.51

Note: Standard deviations of the bond lengths are 0.001.

* TQE (tetrahedral quadratic elongation) = $\Sigma_{i=1}^{4}(l_i/l_o)^2/4$ where l_o is the center-to-vertex distance for a regular tetrahedron whose volume is equal to that of a real tetrahedron with bond lengths l_i. TAV (tetrahedral angle variance) = $\Sigma_{i=1}^{6}(A_i - 109.47)^2/5$ where A_i values are the tetrahedral angles O-T-O. TILT is the out-of-plane tilting of the basal face of the tetrahedra with respect to the plane (100). $TILT_{az}$ is the azimuthal component of the TILT for the two neighboring tetrahedra Si1 and Si2 (equivalent in the *C2/c* symmetry).

TABLE 5b. Mean bond distances (Å) and volumes (Å³) of M1 and M11 polyhedra for *P2/n* pyroxenes

	⟨Si1-O⟩	⟨Si2-O⟩	⟨M11-O⟩	⟨M1-O⟩	⟨M2-O⟩	⟨M21-O⟩	V_{M11}	V_{M1}
74AM40 n.1	1.634(1)	1.633(1)	1.976(1)	2.068(1)	2.477(1)	2.506(1)	10.204	11.600
78AM12 n.2	1.632(1)	1.632(1)	1.974(1)	2.073(1)	2.477(1)	2.508(1)	10.159	11.677
78AM12 n.3	1.633(1)	1.632(1)	1.974(1)	2.073(1)	2.477(1)	2.508(1)	10.159	11.684
74AM41 n.1	1.633(1)	1.631(1)	1.946(1)	2.078(1)	2.472(1)	2.509(1)	9.736	11.730
74AM41 n.2	1.632(1)	1.632(1)	1.945(1)	2.077(1)	2.471(1)	2.508(1)	9.719	11.722
MS1 n.3	1.632(1)	1.631(1)	1.948(1)	2.076(1)	2.470(1)	2.509(1)	9.777	11.706
74AM42 n.1	1.633(1)	1.631(1)	1.945(1)	2.078(1)	2.471(1)	2.510(1)	9.732	11.740
Ma4 n.1	1.630(1)	1.631(1)	1.938(1)	2.079(1)	2.472(1)	2.511(1)	9.619	11.747
Ma4 n.2	1.630(1)	1.629(1)	1.937(1)	2.078(1)	2.470(1)	2.510(1)	9.604	11.728
120853 n.5	1.631(1)	1.630(1)	1.937(1)	2.075(1)	2.470(1)	2.509(1)	9.600	11.680
M106 n.2	1.630(1)	1.630(1)	1.933(1)	2.073(1)	2.469(1)	2.507(1)	9.534	11.640
M106 n.4	1.631(1)	1.630(1)	1.932(1)	2.072(1)	2.469(1)	2.507(1)	9.519	11.614
74AM33 n.11	1.631(1)	1.630(1)	1.932(1)	2.068(1)	2.469(1)	2.507(1)	9.521	11.545
74AM33 n.17	1.630(1)	1.630(1)	1.933(1)	2.070(1)	2.469(1)	2.507(1)	9.545	11.582
74AM33 2.5h	1.631(1)	1.630(1)	1.959(1)	2.040(1)	2.475(1)	2.500(1)	9.908	11.117
74AM33 10h	1.632(1)	1.629(1)	1.978(1)	2.018(1)	2.480(1)	2.493(1)	10.198	10.772
74AM33 45h	1.632(1)	1.629(1)	1.991(1)	2.008(1)	2.481(1)	2.492(1)	10.386	10.637
MfX n.1	1.630(1)	1.629(1)	1.932(1)	2.066(1)	2.469(1)	2.507(1)	9.527	11.512
MfX n.4	1.630(1)	1.630(1)	1.932(1)	2.067(1)	2.469(1)	2.507(1)	9.529	11.524
Br2 n.10	1.630(1)	1.629(1)	1.932(1)	2.070(1)	2.469(2)	2.507(2)	9.525	11.584
Br2 n.11	1.630(1)	1.629(1)	1.931(1)	2.069(1)	2.468(1)	2.506(1)	9.506	11.567
SL988 n.1	1.630(2)	1.629(2)	1.937(2)	2.068(2)	2.471(2)	2.508(2)	9.595	11.559
SL896 n.3	1.630(2)	1.628(2)	1.938(2)	2.052(2)	2.470(2)	2.503(2)	9.608	11.294
SL993 n.1	1.631(2)	1.627(2)	1.939(2)	2.053(2)	2.470(2)	2.502(2)	9.619	11.301

Note: Standard deviations are in parentheses.

tively. Ordered and disordered samples were refined in *P2/n* and *C2/c* space groups, respectively, starting from positional and displacement parameters of pyroxenes of similar composition. No chemical constraints were used. The atomic scattering curves were taken from the *International Tables for X-ray Crystallography* (Ibers and Hamilton 1974) and from Tokonami (1965). Complete ionization of the cations at M1 (Mg^{2+}, Al^{3+}, Fe^{2+}, Fe^{3+}) and M2 (Ca^{2+}, Na^{+}) sites was adopted following Rossi et al. (1983). For O and Si, a series of preliminary refinements were made considering their ionization state as a variable. The results led approximatively to an ionization state of 1.2^- for bridging O, 1.5^- for the other O and 2.2^+ for Si. These values, which ensure charge neutrality, were fixed for further refinements. An extinction parameter, x, in the formula $k[1 + 0.001xF_c^2 \lambda^3/\sin 2\theta]$ (where k is the overall scale factor) was refined. The weighting scheme used is defined as $w = 1/[\sigma^2(F_o^2 + (AP)^2 + BP]$ where P

TABLE 5c. Several geometrical parameters* of tetrahedra Si1 and Si2 for *P2/n* pyroxenes

	TQE Si1	TQE Si2	TAV Si1	TAV Si2	TILT Si1	TILT Si2	$TILT_{az}$ Si1	$TILT_{az}$ Si2	O3(2)-O3(1)-O3(2)
74AM40 n.1	1.0059	1.0055	25.44	23.52	3.023	1.720	163.5	−46.9	168.61
78AM12 n.2	1.0056	1.0054	24.38	22.93	3.085	1.763	161.8	−50.1	168.72
78AM12 n.3	1.0057	1.0054	24.74	22.70	3.077	1.732	162.0	−50.7	168.72
74AM41 n.1	1.0059	1.0052	25.68	22.05	3.491	1.935	156.4	−65.4	168.87
74AM41 n.2	1.0058	1.0053	25.35	22.12	3.450	1.926	156.1	−65.3	168.98
MS1 n.3	1.0059	1.0054	25.67	22.68	3.430	1.909	157.0	−63.3	168.92
74AM42 n.1	1.0058	1.0052	25.42	21.92	3.446	1.911	155.9	−66.9	168.94
Ma4 n.1	1.0058	1.0051	25.36	21.19	3.539	1.977	154.3	−70.2	169.28
Ma4 n.2	1.0059	1.0051	25.81	21.49	3.649	2.003	155.3	−68.5	169.39
120853 n.5	1.0058	1.0051	25.50	21.30	3.517	1.979	154.4	−69.4	169.27
M106 n.2	1.0059	1.0050	25.64	20.91	3.524	1.999	153.2	−71.4	169.55
M106 n.4	1.0058	1.0050	25.39	20.91	3.476	1.956	153.9	−70.3	169.57
74AM33 n.11	1.0058	1.0051	25.37	21.35	3.434	1.917	154.7	−68.7	169.56
74AM33 n.17	1.0058	1.0050	25.20	21.10	3.479	1.948	154.2	−69.9	169.46
74AM33 2.5h	1.0056	1.0053	24.47	22.68	2.739	1.597	163.4	−43.9	169.87
74AM33 10h	1.0056	1.0055	23.91	23.48	2.286	1.668	172.4	−22.3	170.02
74AM33 45h	1.0055	1.0056	23.46	24.00	1.995	1.749	181.6	−8.9	169.97
MfX n.1	1.0057	1.0050	24.71	21.16	3.436	1.954	153.8	−68.7	169.76
MfX n.4	1.0058	1.0050	25.17	21.09	3.408	1.914	154.1	−69.4	169.75
Br2 n.10	10058	1.0049	25.16	20.76	3.471	1.936	153.9	−71.1	169.68
Br2 n.11	1.0058	1.0050	25.20	21.07	3.487	1.968	154.0	−69.5	169.63
SL988 n.1	1.0057	1.0049	24.64	20.77	3.397	1.877	155.6	−65.7	170.00
SL896 n.3	1.0055	1.0050	23.81	21.23	3.068	1.667	157.3	−61.5	170.48
SL993 n.1	1.0056	1.0051	24.31	21.49	3.171	1.810	155.5	−62.9	170.19

* TQE, TAV, TILT, and $TILT_{az}$ as in Table 5a.

FIGURE 3. Compositional dependence of (**a**) unit-cell lattice parameters *a*, *b*, *c* (Å), and angle β (°), and (**b**) unit-cell volume (Å^3). Composition is expressed in this figure and in all the subsequent figures as mole fraction of jadeite + acmite components X_{Jd+Ac}. Filled circles = *C2/c* samples; open circles = *P2/n* samples; filled triangles = experimentally disordered samples; filled squares = synthetic samples. The size of the symbols is on the order of the uncertainties. Only for the unit-cell angle β it is possible to note a difference between ordered and disordered data. Straight lines between the end-members are shown as guides to the eye.

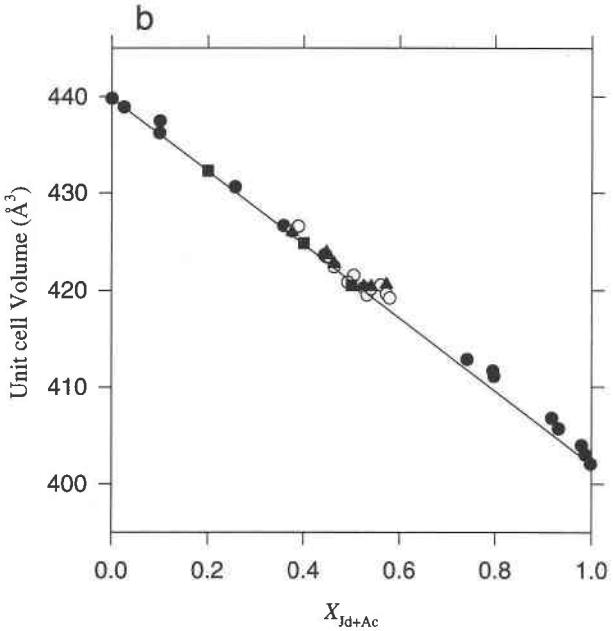

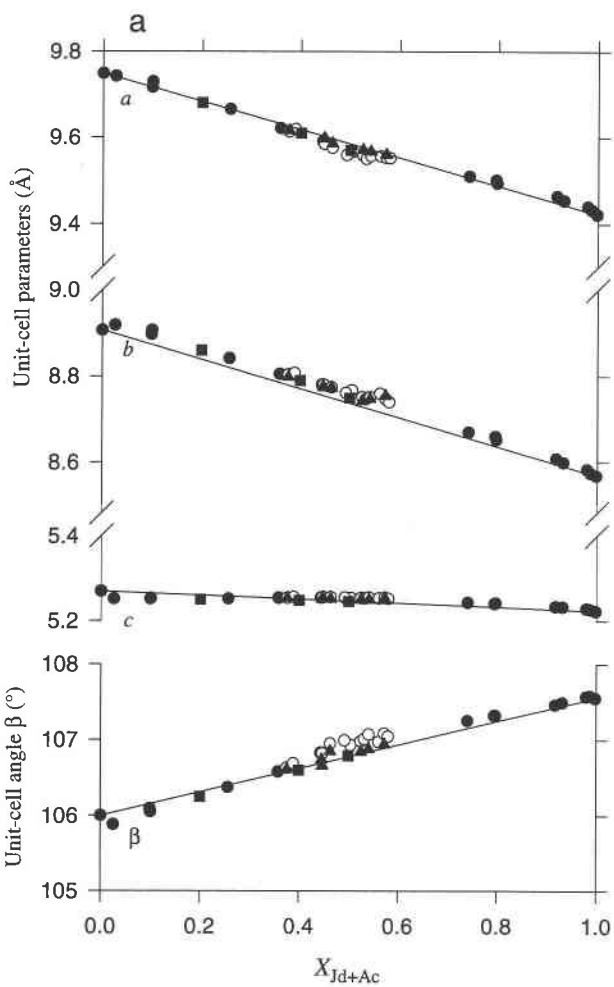

→

= $(F_o^2 + 2F_c^2)/3$. *A* and *B* were chosen for every crystal to produce a flat analysis of variance in terms of F_c^2, as suggested by SHELXL93. All parameters were refined simultaneously, and no correlation greater than 0.69 was observed. For crystals ML n.3, ML n.4, N16/2 n.3, C411g n.1, 74AM43 n.2, and 74AM39 n.1, the Fourier-difference maps revealed the highest residual electron density peak on the diad axis at about 0.68 Å from M2, corresponding to the M2′ site (Rossi et al. 1987). For these crystals, further refinements were therefore made using the Fe^{2+} scattering curve for the isotropic M2′ site and the constraint $X_{Ca}^{M2} + X_{Na}^{M2} + X_{Fe^{2+}}^{M2'} = 1$. The residual electron densities found at the appropriate position for the *C2/c* crystal C413A n.2 and at about 0.62 from the M2 site for five *P2/n* crystals (74AM41 n.1 and n.2, 74AM42

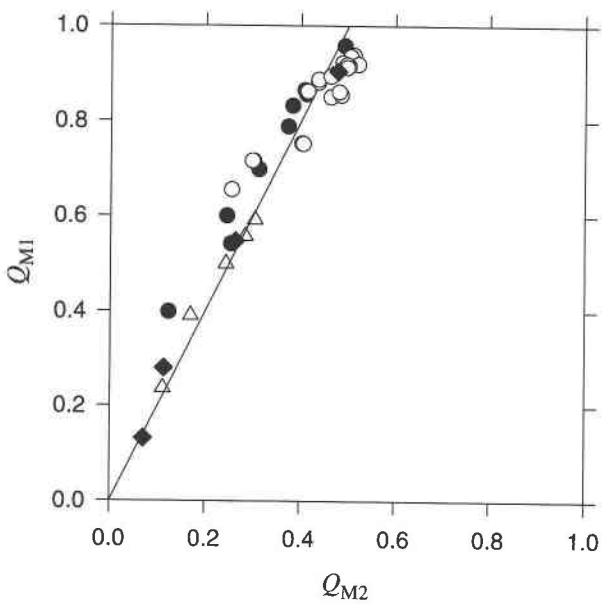

FIGURE 2. Correlation between Q_{M1} and Q_{M2} as determined from average site occupancies for ordered omphacites. Open circles = omphacites investigated in this study; filled diamonds = kinetic experiments of this study; filled circles = Rossi et al. (1983); open triangles = Carpenter et al. (1990a). The data points are consistent, within the uncertainties, with a linear relation $Q_{M1} = 2Q_{M2}$ (straight line).

TABLE 8. Unit-cell constants of the studied pyroxenes from X-ray powder diffraction

	a (Å)	*b* (Å)	*c* (Å)	β (°)	*V* (Å³)
			Natural samples		
ML	9.748(2)	8.906(2)	5.270(1)	106.00(2)	439.77(15)
Diopside	9.742(1)	8.918(1)	5.252(1)	105.88(1)	438.87(11)
N16/2	9.716(1)	8.896(1)	5.252(1)	106.09(1)	436.19(9)
C411	9.729(1)	8.906(1)	5.253(1)	106.05(1)	437.42(8)
74AM43	9.665(1)	8.841(1)	5.252(1)	106.37(1)	430.61(9)
74AM39	9.621(1)	8.805(1)	5.254(1)	106.58(1)	426.58(10)
74AM40	9.613(1)	8.804(1)	5.254(1)	106.63(1)	426.03(10)
78AM12	9.619(1)	8.807(1)	5.256(1)	106.69(1)	426.51(12)
74AM41	9.591(1)	8.780(1)	5.255(1)	106.83(1)	423.60(10)
MS1	9.592(2)	8.780(1)	5.255(1)	106.83(2)	423.60(19)
74AM42	9.585(1)	8.780(1)	5.256(1)	106.82(1)	423.39(8)
Ma4	9.576(2)	8.774(1)	5.256(1)	106.95(1)	422.40(15)
120853	9.566(2)	8.767(1)	5.254(1)	106.93(1)	421.53(14)
M106	9.559(2)	8.761(2)	5.255(1)	106.99(1)	420.83(11)
74AM33	9.558(1)	8.751(1)	5.254(1)	106.98(1)	420.26(12)
MfX	9.550(1)	8.746(1)	5.253(1)	107.01(1)	419.50(10)
Br2	9.557(2)	8.751(1)	5.255(1)	107.07(2)	420.14(16)
SL988	9.556(3)	8.759(2)	5.253(1)	106.97(2)	420.52(19)
SL896	9.553(3)	8.746(2)	5.254(1)	107.08(2)	419.62(20)
SL993	9.552(3)	8.739(2)	5.252(2)	107.04(2)	419.19(25)
C413A	9.510(2)	8.669(1)	5.243(1)	107.25(1)	412.82(16)
C413C	9.501(1)	8.659(1)	5.241(1)	107.32(1)	411.65(8)
C413B	9.494(2)	8.652(1)	5.242(1)	107.32(1)	411.08(15)
SL986	9.464(2)	8.608(1)	5.234(1)	107.46(1)	406.77(17)
SL504	9.454(1)	8.599(2)	5.233(1)	107.49(1)	405.69(11)
SLVD1	9.440(1)	8.583(1)	5.229(1)	107.57(1)	403.95(8)
SL664	9.433(1)	8.574(1)	5.227(1)	107.58(1)	402.99(10)
NI2	9.422(1)	8.568(1)	5.223(1)	107.55(1)	402.04(10)
			Disordered samples		
74AM40 168h	9.616(2)	8.798(1)	5.254(1)	106.61(1)	425.92(15)
MS1 hP	9.597(3)	8.776(1)	5.252(1)	106.74(2)	423.61(16)
74AM42 hP	9.597(3)	8.774(1)	5.254(1)	106.66(2)	423.84(23)
Ma4 hP	9.586(2)	8.773(1)	5.252(1)	106.85(2)	422.72(19)
74AM33 458h	9.571(1)	8.742(1)	5.250(1)	106.84(1)	420.39(9)
Br2 hP	9.567(2)	8.747(1)	5.250(1)	106.88(2)	420.36(15)
SL896 hP	9.560(3)	8.754(2)	5.253(1)	106.94(2)	420.58(26)
			Synthetic samples		
$Di_{80}Jd_{20}$*	9.680(1)	8.859(1)	5.250(1)	106.25(2)	432.27(10)
$Di_{60}Jd_{40}$*	9.610(1)	8.790(1)	5.248(1)	106.60(2)	424.80(19)
$Di_{50}Jd_{50}$*	9.570(1)	8.749(1)	5.246(1)	106.79(2)	420.51(13)

Note: Standard deviations are in parentheses.
* Wood et al. (1980).

n.1, Ma4 n.1, and SL988 n.1) have been neglected because they are very weak.

The number of total and unique reflections I_{tot} and I, the conventional discrepancy indices R, based on $F_o^2 > 2\sigma(F_o^2)$ and wR, based on all the F_o^2, as well as the goodness of fit (S) and refinement data are reported for $C2/c$ and $P2/n$ samples in Table 4a and 4b, respectively. Mean bond distances and other geometrical parameters of the tetrahedra are given in Table 5a for $C2/c$ samples, and in Tables 5b and 5c for $P2/n$ omphacites. The final positional and displacement parameters (Table 6[1]), as well as the observed and calculated structure factors (Table 7[1]) have been deposited.

X-ray powder diffraction

To obtain lattice parameters for all the samples, including those not suitable for single-crystal diffraction, refinements of X-ray powder diffraction data, collected with a focusing Guinier camera and monochromatized Cu$K\alpha_1$ radiation, were performed. Si was used as an internal standard and films were exposed for 3 or 4 d under vacuum to optimize signal-to-background ratios. Individual lines were indexed by following the shifts of the peaks from the end-members augite and jadeite whose reflections are tabulated in Borg and Smith (1969). Up to 35 reflections were used for least-squares refinements. The resulting unit-cell parameters (Table 8) are very close to those determined by X-ray single-crystal diffraction.

SITE POPULATIONS AND LONG-RANGE ORDER PARAMETERS

The site populations of ordered omphacites were determined using both the results of structure refinements and microprobe analysis. The site populations were used to calculate the long-range order parameters Q_{M1} and Q_{M2} for the M1 and M2 sites.

The best value of the atomic fraction X_i^j for each element i at the site j (e.g., M1, M11, M2, and M21 sites) was determined using a minimization procedure based on

TABLE 9. Site distributions and long-range order parameters Q_{M1} and Q_{M2} for *P2/n* pyroxenes

		74AM40 n.1	78AM12 n.2	78AM12 n.3	74AM41 n.1	74AM41 n.2	MS1 n.3	74AM42 n.1	Ma4 n.1	Ma4 n.2	120853 n.5	M106 n.2	M106 n.4
M1	Mg	0.867	0.841	0.843	0.903	0.905	0.933	0.902	0.853	0.831	0.893	0.831	0.832
M1	Al	0.071	0.053	0.055	0.012	0.015	0.018	0.013	0.026	0.041	0.039	0.061	0.067
M1	Fe^{2+}	0.062	0.106	0.102	0.085	0.080	0.049	0.085	0.121	0.128	0.068	0.105	0.101
M1	Fe^{3+}	0.000	0.000	0.000	0.000	0.000	0.000	0.000	0.000	0.000	0.000	0.003	0.000
M11	Mg	0.251	0.230	0.232	0.075	0.077	0.104	0.070	0.016	0.024	0.025	0.019	0.020
M11	Al	0.688	0.666	0.666	0.880	0.885	0.869	0.887	0.922	0.923	0.939	0.944	0.949
M11	Fe^{2+}	0.061	0.032	0.026	0.041	0.035	0.027	0.038	0.020	0.000	0.014	0.000	0.000
M11	Fe^{3+}	0.000	0.072	0.076	0.004	0.003	0.000	0.005	0.042	0.053	0.022	0.037	0.031
Q_{M1}		0.655	0.716	0.716	0.882	0.881	0.862	0.887	0.938	0.935	0.922	0.919	0.915
M2	Ca	0.500	0.461	0.458	0.336	0.332	0.352	0.331	0.249	0.239	0.256	0.217	0.226
M2	Na	0.500	0.539	0.542	0.664	0.668	0.648	0.669	0.751	0.761	0.744	0.783	0.774
M21	Ca	0.740	0.748	0.744	0.767	0.765	0.761	0.764	0.761	0.744	0.744	0.737	0.726
M21	Na	0.260	0.252	0.256	0.233	0.235	0.239	0.236	0.239	0.256	0.256	0.263	0.274
Q_{M2}		0.255	0.301	0.298	0.436	0.437	0.414	0.437	0.512	0.505	0.488	0.521	0.501
							Atoms p.f.u.						
Si		2.000	2.000	2.000	2.000	2.000	2.000	2.000	2.000	2.000	2.000	2.000	2.000
Mg		0.559	0.536	0.537	0.489	0.491	0.518	0.486	0.435	0.428	0.459	0.425	0.426
Al		0.380	0.359	0.361	0.446	0.450	0.444	0.450	0.474	0.482	0.489	0.502	0.508
Fe^{2+}		0.061	0.069	0.064	0.063	0.058	0.038	0.062	0.070	0.064	0.041	0.053	0.050
Fe^{3+}		0.000	0.036	0.038	0.002	0.001	0.000	0.002	0.021	0.026	0.011	0.020	0.016
Ca		0.620	0.605	0.601	0.552	0.549	0.556	0.548	0.505	0.492	0.500	0.477	0.476
Na		0.380	0.395	0.399	0.448	0.451	0.444	0.452	0.495	0.508	0.500	0.523	0.524

the MINUIT program library (James and Ross 1975). The quantity minimized was

$$M = (wR)^2 = \sum \left[\left(1 - \frac{P_{cal}}{P_{obs}} \right) \Big/ \frac{\sigma(P_{obs})}{P_{obs}} \right]^2,$$

i.e., the weighted sum of squares of residuals R between observed and calculated values of chemical and structural parameters P. The weight, w, is inversely proportional to the observed standard deviation σ. The structural parameters are the mean atomic number (m.a.n.) at the M1, M11, M2, and M21 sites and the mean bond distances ⟨M1-O⟩ and ⟨M11-O⟩ from the structure refinements. The relevant residuals were calculated as follows:

$$R_1 = 1 - (12X_{Mg}^{M1} + 13X_{Al}^{M1} + 26X_{Fe^{2+}}^{M1} + 26X_{Fe^{3+}}^{M1}) \div \text{m.a.n.}^{M1}. \quad (1)$$

TABLE 9—*Continued*

		74AM33 n.11	74AM33 n.17	74AM33 2.5 h	74AM33 10 h	74AM33 45 h	MfX n.1	MfX n.4	Br2 n.10	Br2 n.11	SL988 n.1	SL896 n.3	SL993 n.1
M1	Mg	0.824	0.835	0.671	0.552	0.488	0.764	0.764	0.804	0.800	0.674	0.530	0.578
M1	Al	0.089	0.085	0.265	0.401	0.471	0.132	0.126	0.086	0.092	0.125	0.251	0.241
M1	Fe^{2+}	0.087	0.080	0.057	0.045	0.041	0.104	0.110	0.110	0.108	0.201	0.219	0.181
M1	Fe^{3+}	0.000	0.000	0.007	0.002	0.000	0.000	0.000	0.000	0.000	0.000	0.000	0.000
M11	Mg	0.010	0.005	0.146	0.266	0.337	0.000	0.000	0.002	0.003	0.006	0.000	0.024
M11	Al	0.973	0.977	0.800	0.669	0.590	0.973	0.972	0.974	0.973	0.935	0.939	0.924
M11	Fe^{2+}	0.011	0.010	0.039	0.053	0.062	0.027	0.028	0.000	0.000	0.017	0.032	0.014
M11	Fe^{3+}	0.006	0.008	0.015	0.012	0.011	0.000	0.000	0.024	0.024	0.042	0.029	0.038
Q_{M1}		0.894	0.904	0.547	0.280	0.131	0.850	0.854	0.918	0.912	0.861	0.753	0.752
M2	Ca	0.236	0.227	0.326	0.402	0.429	0.219	0.211	0.211	0.208	0.211	0.199	0.205
M2	Na	0.764	0.773	0.674	0.598	0.571	0.781	0.789	0.789	0.792	0.789	0.801	0.795
M21	Ca	0.697	0.703	0.587	0.514	0.499	0.677	0.691	0.704	0.702	0.687	0.582	0.593
M21	Na	0.303	0.297	0.413	0.486	0.501	0.323	0.309	0.296	0.298	0.313	0.418	0.407
Q_{M2}		0.463	0.478	0.263	0.113	0.070	0.463	0.485	0.497	0.498	0.481	0.402	0.405
							Atoms p.f.u.						
Si		2.000	2.000	2.000	2.000	2.000	2.000	2.000	2.000	2.000	2.000	2.000	2.000
Mg		0.417	0.420	0.409	0.409	0.413	0.382	0.382	0.403	0.401	0.340	0.265	0.301
Al		0.531	0.531	0.532	0.535	0.530	0.552	0.549	0.530	0.533	0.530	0.595	0.582
Fe^{2+}		0.049	0.045	0.048	0.049	0.051	0.066	0.069	0.055	0.054	0.109	0.125	0.098
Fe^{3+}		0.003	0.004	0.011	0.007	0.006	0.000	0.000	0.012	0.012	0.021	0.015	0.019
Ca		0.466	0.465	0.457	0.458	0.464	0.448	0.451	0.458	0.455	0.449	0.390	0.399
Na		0.534	0.535	0.543	0.542	0.536	0.552	0.549	0.542	0.545	0.551	0.610	0.601

Note: Estimated error ranges for the site occupancies: 0.007–0.009 (Mg and Al); 0.008–0.01 (Fe^{2+} and Fe^{3+}); 0.005–0.007 (Ca and Na). Si is assumed to be 2.000 apfu.

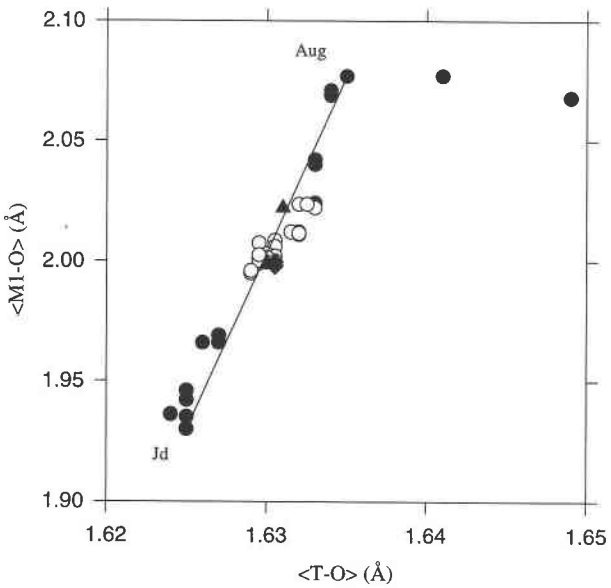

FIGURE 4. Plot of octahedral mean bond distances ⟨M1-O⟩ against tetrahedral mean bond distances ⟨T-O⟩. The departure from linearity is caused by Al entering the tetrahedra for the two single crystals of sample ML. For ordered omphacites ⟨M1-O⟩ = (⟨M1-O⟩ + ⟨M11-O⟩)/2 and ⟨T-O⟩ = (⟨T1-O⟩ + ⟨T11-O⟩)/2. Filled circles = *C2/c* samples; open circles = *P2/n* omphacites; filled triangles = experimentally disordered (*C2/c*) samples; filled diamonds = progressively disordered 74AM33 crystals.

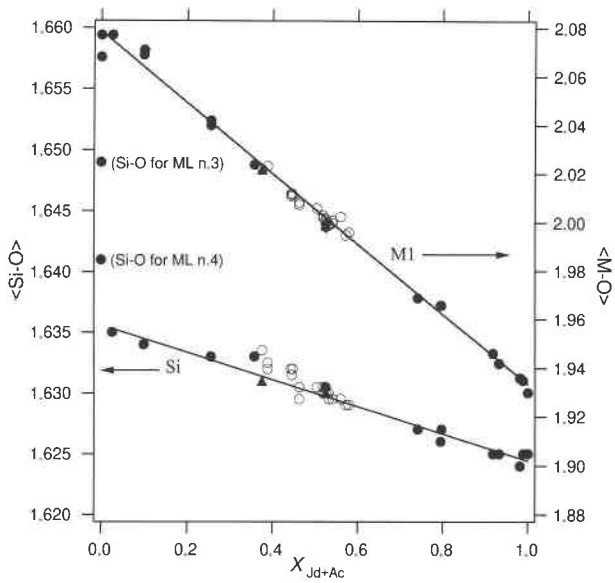

FIGURE 5. Variation of the tetrahedral and octrahedral (right-hand axis) mean bond distances as a function of composition. For ordered samples ⟨Si-O⟩ = (⟨Si1-O⟩ + ⟨Si2-O⟩)/2 and ⟨M1-O⟩ = (⟨M1-O⟩ + ⟨M11-O⟩)/2. The two data points at $X_{Jd+Ac} = 0$ which fall off the linear trend correspond to the single crystals of sample ML with $^{[4]}$Al. Symbols as in Figure 4. Note that there is no difference between ordered and annealed omphacites.

$$R_2 = 1 - (12X_{Mg}^{M11} + 13X_{Al}^{M11} + 26X_{Fe^{2+}}^{M11} + 26X_{Fe^{3+}}^{M11}) \div \text{m.a.n.}^{M11}. \quad (2)$$

$$R_3 = 1 - (20X_{Ca}^{M2} + 11X_{Na}^{M2})/\text{m.a.n.}^{M2}. \quad (3)$$

$$R_4 = 1 - (20X_{Ca}^{M21} + 11X_{Na}^{M21})/\text{m.a.n.}^{M21}. \quad (4)$$

$$R_{11} = 1 - (2.077X_{Mg}^{M1} + 1.928X_{Al}^{M1} + 2.130X_{Fe^{2+}}^{M1} + 2.025X_{Fe^{3+}}^{M1})/\langle M1\text{-}O\rangle_{obs}. \quad (5)$$

$$R_{12} = 1 - (2.077X_{Mg}^{M11} + 1.928X_{Al}^{M11} + 2.130X_{Fe^{2+}}^{M11} + 2.025X_{Fe^{3+}}^{M11})/\langle M11\text{-}O\rangle_{obs}. \quad (6)$$

In Equations 1, 2, 3, and 4, the coefficients of the atomic fractions X_i are the atomic numbers of the elements that occur at the sites M1, M11, M2, and M21, respectively. In Equations 5 and 6, the coefficients are the mean ⟨M1-O⟩ bond distances in pure diopside, jadeite, hedenbergite, and acmite, respectively (Cameron and Papike 1981).

The chemical parameters considered were the atomic fractions of Al, Mg, Fe^{2+}, Fe^{3+}, Ca, and Na as determined by microprobe analysis. The other elements (Ti, Cr, Mn, and K) were ignored because they never exceeded 0.005 atoms per formula unit (apfu) and their sum never exceeded 0.009 apfu in the analyzed crystals. For sample 74AM40, Cr is 0.007 apfu and the sum of the ignored elements is 0.011 apfu, but their concentrations (other than Cr) are smaller than the experimental uncertainty for these elements. The chemical residual calculated for Mg is

$$R_5 = 1 - \left(\frac{1}{2}X_{Mg}^{M11} + \frac{1}{2}X_{Mg}^{M1}\right) \Big/ \text{Mg(apfu)}. \quad (7)$$

The residuals R_6 to R_{10} were calculated as R_5 for the other isomorphous elements at the M1 and M11 sites (Al, Fe^{2+} and Fe^{3+}) and for Na and Ca at the M2 and M21 sites. In the minimization procedure, the following constraints were adopted: (1) All the structural sites were considered to be fully occupied. (2) Electroneutrality was ensured by the constraints:

$$X_{Ca}^{M21} + X_{Ca}^{M2} = X_{Mg}^{M11} + X_{Mg}^{M1} + X_{Fe^{2+}}^{M11} + X_{Fe^{2+}}^{M1}$$

$$X_{Na}^{M21} + X_{Na}^{M2} = X_{Al}^{M11} + X_{Al}^{M1} + X_{Fe^{3+}}^{M11} + X_{Fe^{3+}}^{M1}.$$

(3) Fe^{2+} and Fe^{3+} were partitioned in the same way as Mg and Al, respectively. (4) The tetrahedral site is filled with Si. The resulting site occupancies are given in Table 9.

For ordered omphacites, the degree of order over M1 and M2 sites is expressed through the order parameters Q_{M1} and Q_{M2} (Carpenter et al. 1990a) as

$$Q_{M1} = \left(\left|\frac{(Al + Fe^{3+})_{M1} - (Al + Fe^{3+})_{M11}}{\Sigma(Al + Fe^{3+})}\right| + \left|\frac{(Mg + Fe^{2+})_{M1} - (Mg + Fe^{2+})_{M11}}{\Sigma(Mg + Fe^{2+})}\right|\right) \Big/ 2.$$

$$Q_{M2} = \left(\left|\frac{Na_{M2} - Na_{M21}}{\Sigma Na}\right| + \left|\frac{Ca_{M2} - Ca_{M21}}{\Sigma Ca}\right|\right) \Big/ 2.$$

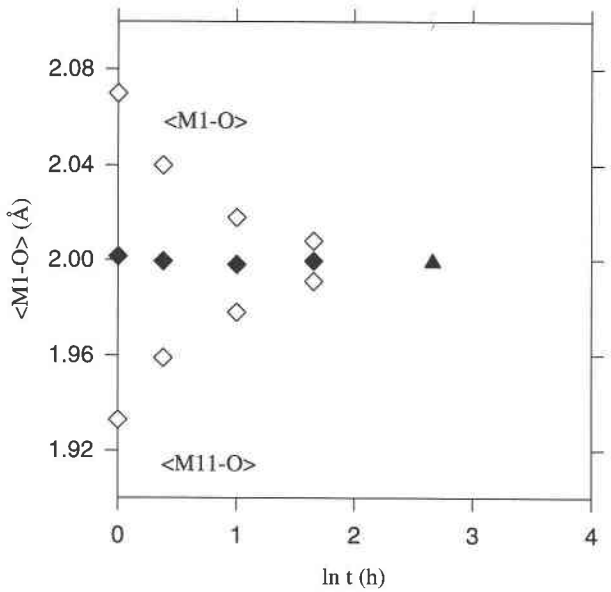

FIGURE 6. Variation of the ⟨M1-O⟩ and ⟨M11-O⟩ octahedral mean bond distances of the progressively disordered crystals of sample 74AM33 as a function of annealing time. The natural *P2/n* crystal 74AM33 n.17 is shown at ln(t) = 0 for comparison. Open diamonds = ⟨M1-O⟩ and ⟨M11-O⟩ mean bond distances; filled diamonds = average value (⟨M1-O⟩+⟨M11-O⟩)/2; filled triangle = ⟨M1-O⟩ mean bond distances of the completely disordered omphacite. Note that the average value remains practically constant during the annealing experiments.

The resulting long-range order parameters (Table 9) are shown in Figure 2. The new data are consistent with the linear correlation between Q_{M1} and Q_{M2} described by Carpenter et al. (1990a) and with the observation that even the most ordered samples are only partially ordered at the M2 sites. Crystals of sample 74AM33 annealed for different times at high temperature follow the same trend as the single crystal experimentally disordered by Carpenter et al. (1990a).

RESULTS AND DISCUSSION

Changes in the geometrical parameters induced by variations in composition and degree of order in the system Aug-Jd give a complete description of the macroscopic behavior of this solid solution. The unit-cell parameters of both ordered (*P2/n*) and disordered (natural and annealed *C2/c*) crystals show a linear trend from Aug to Jd (Figs. 3a and 3b); only for the angle β (Fig. 3a) is the difference between the values of ordered and disordered omphacites larger than the estimated standard deviations ($\Delta\beta \geq 5$ esd). Any macroscopic strain related to the phase transition *C2/c* ↔ *P2/n* is very small (≤ 0.001).

The correlation between octahedral and tetrahedral bond distances is shown in Figure 4. For ordered omphacites, ⟨M1-O⟩ is the average of ⟨M11-O⟩ and ⟨M1-O⟩,

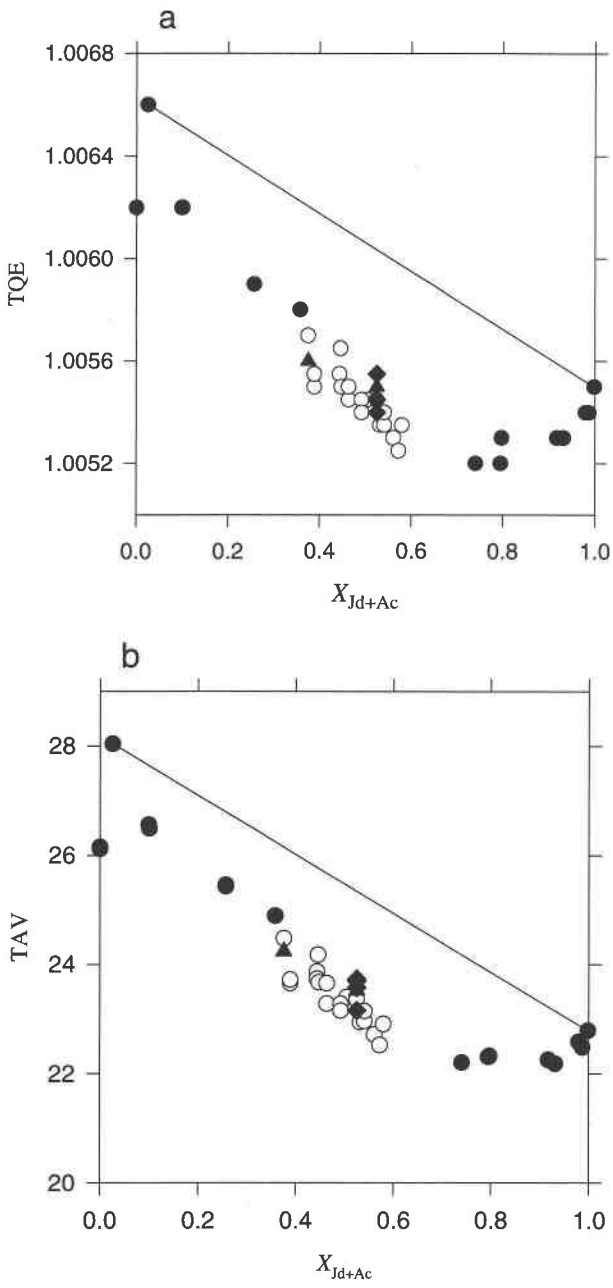

FIGURE 7. Variation as a function of composition of (**a**) tetrahedral quadratic elongation (TQE), and (**b**) tetrahedral angle variance (TAV). For ordered samples: TQE = [TQE(Si1) + TQE(Si2)]/2 and TAV = [TAV(Si1) + TAV(Si2)]/2. Symbols as in Figure 4. The straight line representing the ideal behavior of the solid solution Aug-Jd does not take into account the data at $X_{Jd+mAc} = 0$ corresponding to the sample ML with tetrahedral Al. Note that *P2/n* average values and *C2/c* data plot on the same trend.

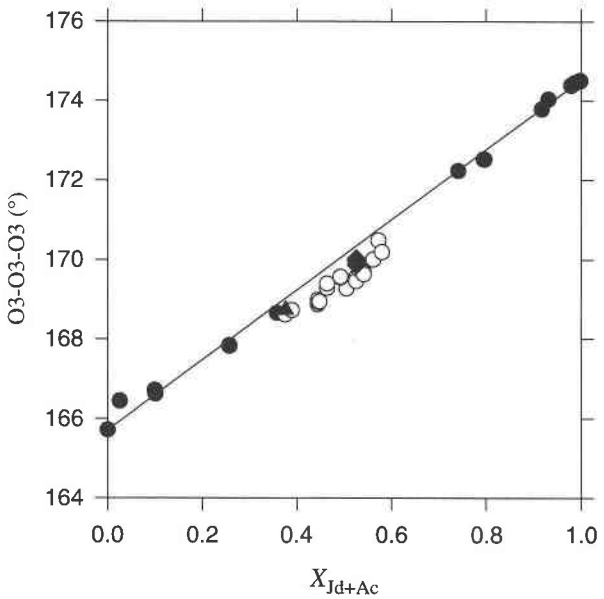

FIGURE 8. Variation as a function of composition of the straightening of the tetrahedral chains expressed as O3-O3-O3 angle [O3(2)-O3(1)-O3(2) angle for ordered omphacites]. Symbols as in Figure 4. This suggests that tetrahedral chains are relatively rigid along their lengths. A straight line between the end-members is shown as guide to the eye.

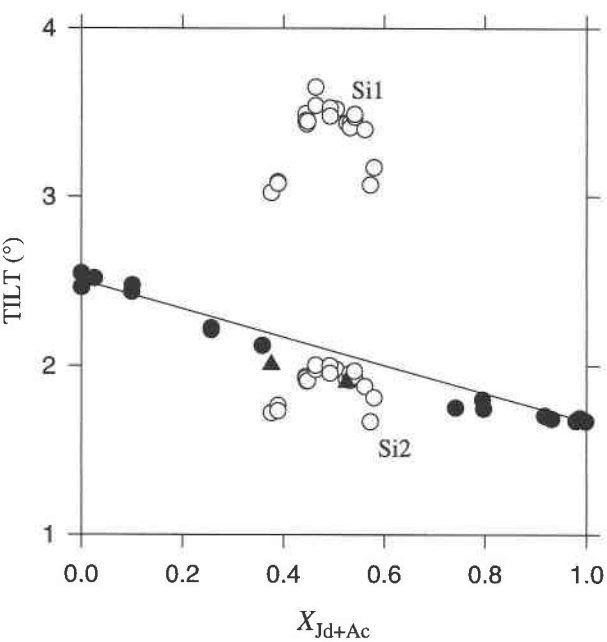

FIGURE 9. Variation as a function of composition of the out-of-plane tilting of the basal face of tetrahedra (TILT). Filled circles = *C2/c* samples; open circles = TILT of both Si1 and Si2 tetrahedra; filled triangles = experimentally disordered (*C2/c*) samples. Note that the TILT values of the Si1 tetrahedra are responsible for the departure of the *P2/n* data from the curve of the TILT of the *C2/c* samples. A straight line between the end-members is shown as guide to the eye.

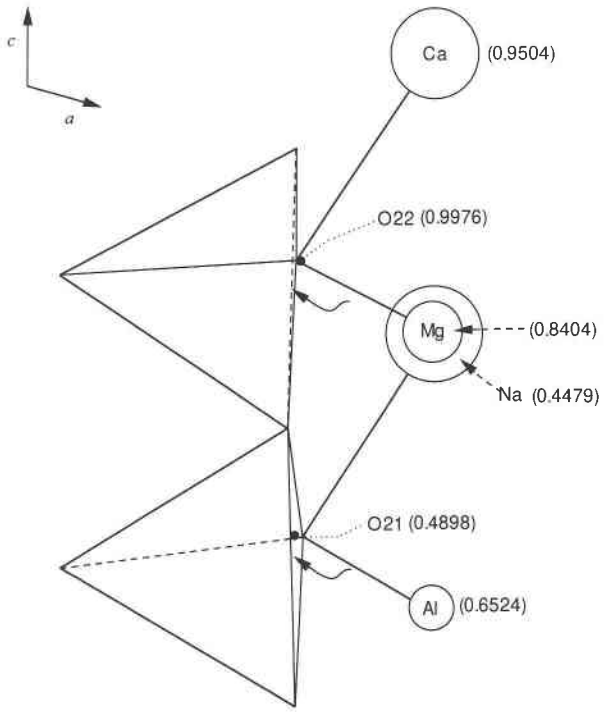

FIGURE 10. Projection of the structure of the natural ordered (*P2/n*) crystal 74AM33 n.17 on the *a-c* plane. The numbers denote the fractional *y/b* coordinate of the atoms. The small differences between the positions of the O21 atom related to Al and Na and the O22 atom related to Mg and Ca with respect to the positions of the O atoms in the *C2/c* omphacite (denoted by the two black dots) determine the change in the TILT values between ordered and disordered samples (if the TILT value was zero, the bases of the tetrahedra indicated by the arrows would be normal to the plane of the diagram). Note that the Si1 tetrahedron is more affected by the cation ordering.

and ⟨T-O⟩ is the average of ⟨Si1-O⟩ and ⟨Si2-O⟩ distances. The tetrahedral bond distances in pyroxenes depend on the $^{[4]}$Al content and on the radius of the cations present at M1 and M2 sites (Rossi et al. 1983). Only the two single crystals of sample ML fall off the line connecting $^{[4]}$Al-free Di and Jd (Fig. 4), showing that this sample contains Al at the T sites. For all the other samples, the Al content of the chemical analyses was considered to be completely $^{[6]}$Al.

As well as the unit-cell parameters, tetrahedral and octahedral mean bond distances for both *C2/c* and *P2/n* samples vary practically linearly with composition along the join Aug-Jd (Fig. 5). Note the two points that fall off the linear trend in Figure 5 correspond to the two crystals of sample ML with tetrahedral Al. The progressive variation of ⟨M1-O⟩ and ⟨M11-O⟩ of the experimentally disordered crystals of sample 74AM33 as a function of the annealing time is shown in Figure 6. ⟨M11-O⟩ increases and ⟨M1-O⟩ decreases with decreasing degree of order, such that their average remains constant at the value of the disordered *C2/c* crystal.

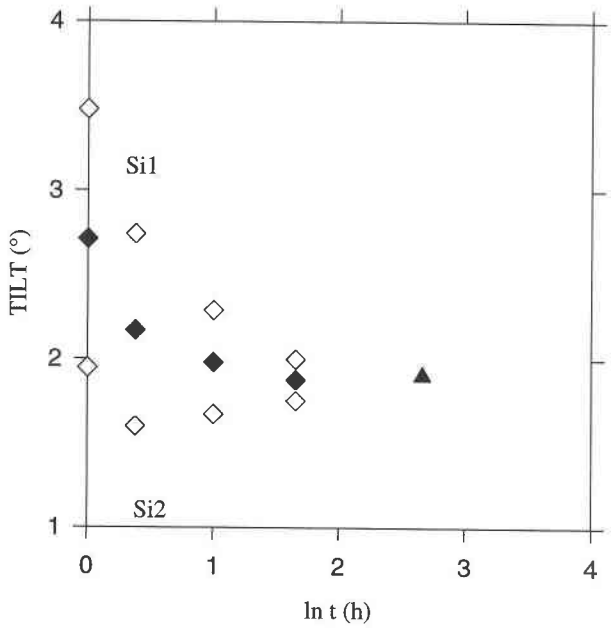

FIGURE 11. Variation of the out-of-plane tilting TILT as a function of annealing time. The natural *P2/n* crystal 74AM33 n.17 is shown at ln(t) = 0 for comparison. Filled diamonds = average ⟨TILT⟩ for the progressively annealed samples; open diamonds = TILT of the Si1 and Si2 tetrahedra; filled triangle = completely disordered (*C2/c*) crystal. Si1 and Si2 tetrahedra show a different behavior during the annealing experiments.

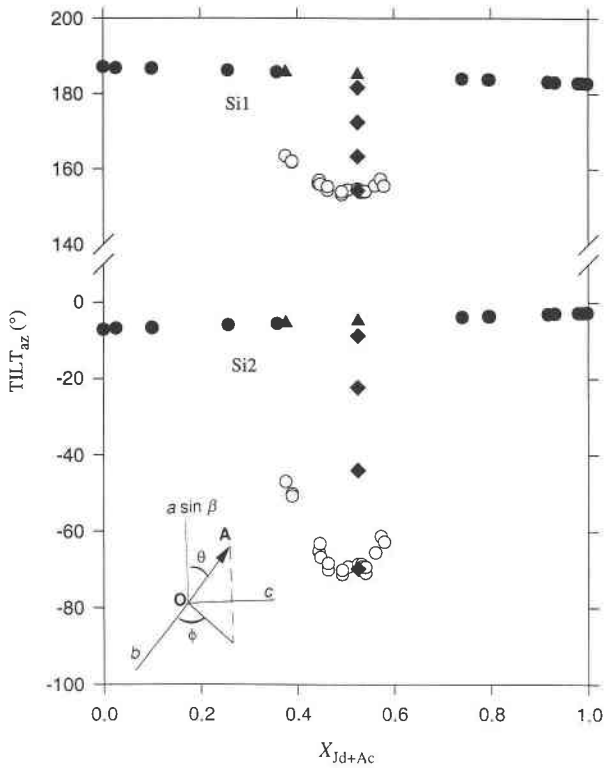

FIGURE 12. The unit vector $\overline{OA}$ normal to the tetrahedral face corresponds to the out-of-plane tilting of the basal face of the tetrahedra with respect to the *b-c* plane in polar coordinates, and it is given in terms of zenithal angle θ (TILT) and azimuthal angle ϕ (TILT$_{az}$). The variation of the azimuthal component of the out-of-plane tilting TILT$_{az}$ is shown as a function of composition for the two neighboring tetrahedra Si1 and Si2 (equivalent in *C2/c* samples). Symbols as in Figure 4. Note the continuous variation of the kinetic data of sample 74AM33 to reach the value of the completely disordered omphacite.

In contrast, the tetrahedral distortion parameters, expressed as tetrahedral quadratic elongation (TQE) and tetrahedral angle variance (TAV) (Robinson et al. 1971) depend non-linearly on composition (Figs. 7a and 7b). The straight line representing the ideal behavior of the solid solution Aug-Jd does not take into account the data at $X_{Jd+Ac} = 0$, corresponding to the sample ML with $^{[4]}$Al. The deviation from linearity is also asymmetric in the same sense as the observed enthalpy of mixing for the solid solution (Wood et al. 1980). In *P2/n* samples, the TQE and TAV values of the Si1 tetrahedra are larger than those of the Si2 tetrahedra (Table 5c). Note, however, that the average data for ordered crystals (natural and progressively disordered) plot on the same trend as the *C2/c* crystals, suggesting that the non-linearity may not be directly related to the non-ideality of the *C2/c* solid solution.

Two more parameters, the kinking angle O3-O3-O3 and the out-of-plane tilting TILT (Cameron et al. 1973), describe the way in which the tetrahedral chains accommodate changes in composition and degree of order. The kinking angle O3-O3-O3, related to the straightening of the tetrahedral chains (Fig. 8), shows a nearly linear correlation with composition without any difference between ordered and disordered samples. The out-of-plane tilting (TILT) of the basal face of the tetrahedra, related to the way octahedra and tetrahedra accommodate each other, is remarkably sensitive to the ordering process. As already observed by Rossi et al. (1983), the average TILT values for Si1 and Si2 tetrahedra of *P2/n* samples do not fall on the curve of the *C2/c* pyroxenes (whose data also show a small deviation from linearity at intermediate compositions). The departure of the *P2/n* average TILT values from the *C2/c* data depends only on the Si1 tetrahedra, because the TILT values of the Si2 tetrahedra are close to those of the *C2/c* samples (Fig. 9). This effect is visible in Figure 10 where the structure of the natural *P2/n* omphacite 74AM33 is shown in the *a-c* plane. The ordering process causes a small rotation of the tetrahedra in opposite directions with respect to the analogous positions in *C2/c* omphacite. Although the changes for both tetrahedra are very small, this effect is greater for the O21 atom coordinated to the M11 site (Al-rich) than for the O22 atom coordinated to the M1 site (Mg-rich). The difference in the TILT values of the Si1 and Si2 tetrahedra may be due mainly to the difference in the radii of Al and Mg that order at the M1 sites. The changes in the

TILT data during the disordering process of the crystals of sample 74AM33 are shown in Figure 11. The average TILT values of the Si1 and Si2 tetrahedra decrease with decreasing degree of order until they reach the value of completely disordered (*C2/c*) omphacite. Whereas the TILT of Si1 tetrahedra decreases rapidly during the annealing process, the TILT of the Si2 tetrahedra initially decreases, then increases to the disordered value. To characterize more precisely the out-of-plane tilting of the basal face of the tetrahedra with respect to the (100) plane, another angular parameter has been measured. This parameter, called here $TILT_{az}$, expresses the azimuthal component of the TILT. The values of $TILT_{az}$ have been calculated, for both *P2/n* and *C2/c* samples for the two neighboring tetrahedra, Si1 and Si2 (which are equivalent in *C2/c* symmetry). The variation of the $TILT_{az}$ data as a function of composition is shown in Figure 12. The $TILT_{az}$ values of both tetrahedra are nearly unaffected by the composition for the *C2/c* samples, but are very sensitive to the degree of order. $TILT_{az}$ of Si1 and Si2 tetrahedra have qualitatively the same pattern, however the difference between ordered and disordered samples is larger for the Si2 tetrahedra.

Acknowledgments

The authors thank R. Bocchio, R. Compagnoni, T. Holland, B. Lombardo, C. Malgarotto, and R.Tribuzio for supplying most of the pyroxenes samples, and F. Hawthorne and G. Harlow for their reviews of the manuscript. Financial support was provided by the CNR (Centro di Studio per la Cristallochimica e la Cristallografia, Pavia) and by MURST (grant 40% V. Tazzoli).

References cited

Aurisicchio, C., Bocchio, R., Liborio, G., and Mottana, A. (1985) Petrogenesis of the eclogites from Soazza, Switzerland. Chemical Geology, 50, 47–63.

Blessing, R.H., Coppens, P., and Becker, P. (1974) Computer analysis of step-scanned X-ray data. Journal of Applied Crystallography, 7, 488–492.

Boffa Ballaran, T. and Domeneghetti, M.C. (1996) Crystal-chemistry and order parameters of Sesia-Lanzo and Dora-Maira omphacites. Bollettino del Museo Regionale di Scienze Naturali, Supplemento al Volume 13, 273–292.

Boffa Ballaran, T., Carpenter, M.A., Domeneghetti, M.C., Salje, E.K.H., and Tazzoli, V. (1998) Structural mechanisms of solid solution and cation ordering in augite-jadeite pyroxenes: II. A microscopic perspective. American Mineralogist, 83, 434–443.

Borg, I.Y. and Smith, D.K. (1969) Calculated X-ray powder patterns for silicate minerals. Geological Society of America Memoir, 122, 238–245 and 269–271.

Burton, B.P. and Davidson, P.M. (1988a) Order-disorder in omphacitic pyroxenes: A model for coupled substitution in the point approximation—Reply. American Mineralogist, 73, 916–918.

———(1988b) Short-range order and frustration in omphacite: Comparison of three CVM approximations. Physics and Chemistry of Minerals, 15, 570–578.

Cameron, M. and Papike, J.J. (1981) Structural and chemical variations in pyroxenes. American Mineralogist, 66,1–50.

Cameron, M., Sueno, S., Prewitt, C.T., and Papike, J.J. (1973) High temperature crystal chemistry of acmite, diopside, hedenbergite, jadeite, spodumene, and ureyite. American Mineralogist, 58, 594–618.

Cannillo, E., Germani, G., and Mazzi, F. (1983) New crystallographic software for Philips PW 1100 single crystal diffractometer. CNR Centro di Studio per la Cristallografia, Internal Report 2.

Carpenter, M.A. (1980) Mechanisms of exsolution in sodic pyroxenes. Contributions to Mineralogy and Petrology, 71, 289–300.

———(1981) Time-temperature-transformation (TTT) analysis of cation disordering in omphacite. Contributions to Mineralogy and Petrology, 78, 433–440.

———(1983) Microstructures in sodic pyroxenes: implications and applications. Periodico di Mineralogia-Roma, 52, 271–301.

Carpenter, M.A., Domeneghetti, M.C., and Tazzoli, V. (1990a) Application of Landau theory to cation ordering in omphacite I: Equilibrium behaviour. European Journal of Mineralogy, 2, 7–18.

———(1990b) Application of Landau theory to cation ordering in omphacite II: Kinetic behaviour. European Journal of Mineralogy, 2, 19–28.

Coleman, R.G. (1961) Jadeite deposits of the Clear Crek area, New Idria District, San Benito County, California. Journal of Petrology, 2, 209–247.

Davidson, P.M. and Burton, B.P. (1987) Order-disorder in omphacitic pyroxenes: A model for coupled substitution in the point approximation. American Mineralogist, 72, 337–344.

Gasparik, T. (1985) Experimentally determined compositions of diopside-jadeite pyroxene in equilibrium with albite and quartz at 1200–1350 °C and 15–34 kbar. Geochimica et Cosmochimica Acta, 49, 865–870.

Holland, T.J.B. (1983) The experimental determination of activities in disordered and short-range ordered jadeitic pyroxenes. Contributions to Mineralogy and Petrology, 82, 214–220.

———(1990) Activities of components in omphacitic solid solutions An application of Landau theory to mixtures. Contributions to Mineralogy and Petrology, 105, 446–453.

Ibers, J.A. and Hamilton, W.C., Eds. (1974) International tables for X-ray crystallography, Vol. IV, 366p. Kynoch, Birmingham, U.K.

Kienast, J.R., Lombardo, B., Biino, G., and Pinardon, L. (1991) Petrology of very-high-pressure eclogitic rocks from the Brossasco-Isasca Complex, Dora-Maira Massif, Italian Western Alps. Journal of Metamorphic Geology, 9, 19–34.

James, F. and Ross, M. (1975) MINUIT, a system for function minimisation and analysis of the parameter errors and correlations. CERN/DD, Internal Report 75/20, Computer Physics, 10, 343–347.

Lappin, M.A. and Smith, D.C. (1978) Mantle-equilibrated orthopyroxenes eclogite pods from the basal gneisses in the Selje District, Western Norway. Journal of Petrology, 19, 530–584.

Lehmann, M.S. and Larsen, F.K. (1974) A method for the location of the peaks in step-scan measured Bragg reflections. Acta Crystallographica, A30, 580–584.

Lombardo, B., Compagnoni, R., Fiora, L., and Facchinelli, A. (1977) Composition of some sodic pyroxenes from the eclogitic micaschists of lower Val d'Aosta (Sesia Lanzo zone, Western Alps). Rendiconti Società Italiana Mineralogia e Petrografia, 33, 375–387.

Matthes, S. and Schmidt, K. (1974) Eclogites of the Münchberg Mass, NE Bavaria. Fortschritte der Mineralogie, 52, 33–57.

Medaris, L.G., Jr. (1980) Petrogenesis of the Lien peridote and associated eclogites, Almklovdalen, Western Norway. Lithos, 13, 339–353.

North, A.C.T., Phillips, D.C., and Mathews, F.S. (1968) A semi-empirical method of absorption correction. Acta Crystallographica, A24, 351–359.

Robinson, K., Gibbs, G.V., and Ribbe, P.H. (1971) Quadratic elongation, a quantitative measure of distortion in co-ordination polyhedra. Science, 172, 567–570.

Rossi, G., Smith, D.C., Ungaretti, L., and Domeneghetti, M.C. (1983) Crystal-chemistry and cation ordering in the system diopside-jadeite: A detailed study by crystal structure refinement. Contributions to Mineralogy and Petrology, 83, 247–258.

Rossi, G., Oberti, R., Dal Negro, A., Molin, G.M., and Mellini, M. (1987) Residual electron density at the M2 site in *C2/c* clinopyroxene: relationships with bulk chemistry and sub-solidus evolution. Physics and Chemistry of Minerals, 14, 514–520.

Stoppa, F. and Lavecchia, G. (1992) Late Pleistocene ultra-alkaline mag-

matic activity in the Umbria-Latium region (Italy): an overview. Journal of Vulcanology and Geothermal Research, 52, 277–293.

Sheldrick, G.M. (1993) SHELXL93. Program for crystal structure refinement. University of Göttingen, Germany.

Tokonami, M. (1965) Atomic scattering factors for O^{2-}. Acta Crystallographica, 19, 486.

Ungaretti, L., Lombardo, B., Domeneghetti, M.C., and Rossi, G. (1983) Crystal-chemical evolution of amphiboles from eclogitised rocks of the Sesia-Lanzo Zone, Italian Western Alps. Bulletin de la Mineralogie, 106, 645–672.

Wood, B.J., Holland, T.J.B., Newton, R.C., and Kleppa, O.J. (1980) Termochemistry of jadeite-diopside pyroxenes. Geochimica et Cosmochimica Acta, 44, 1363–1371.

Manuscript received February 12, 1997
Manuscript accepted October 9, 1997
Paper handled by George A. Lager